RSC Advances

PAPER

View Article Online
View Journal | View Issue

Cite this: *RSC Adv.*, 2014, **4**, 44117

Vegetable-extracted carbon dots and their nanocomposites for enhanced photocatalytic H_2 production

Jing Wang,[a] Yeow Hwee Ng,[b] Yee-Fun Lim[c] and Ghim Wei Ho*[ab]

Received 18th July 2014
Accepted 29th August 2014

DOI: 10.1039/c4ra07290a

www.rsc.org/advances

In this work, we describe a facile construction of eco-friendly and effective nanocomposites from carbon dots (CDs), a novel type of carbon nanomaterial, for photocatalytic purposes. A series of benign CDs with favourable photoluminescence (PL) features were initially obtained from the hydrothermal treatment of natural vegetables including guava, red pepper, peas and spinach. The spinach-extracted CDs, with the highest PL emission intensity, were integrated with versatile TiO_2 ensembles, *i.e.* nanoparticles (NPs) and nanotubes (NTs), to form desirable nanocomposites by further hydrothermal synthesis. TEM images, coupled with XPS spectra, confirm that the CDs are well decorated on the surfaces of TiO_2. Due to the favourable electron transfer property of CDs, the H_2 generation rates are enhanced to 75.5 and 246.1 μmol g^{-1} h^{-1} for TiO_2 NP/CD and NT/CD nanocomposites, which are 21.6 and 3.3 times the rates of bare NPs and NTs, respectively. The strategy reported here may contribute to the fabrication of green and efficient nanocomposites for diverse applications.

Introduction

The pursuit of inexpensive, eco-friendly and efficient nanocomposites has received great interest due to their multiphasic properties from distinct compositions.[1–3] Labelled as non-toxic and biocompatible, fluorescent carbon dots (CDs), a novel type of carbon nanomaterial with sizes below 10 nm, have received increasing attention within the past few years.[4–6] To date, several CD-based nanocomposites have been achieved, including the inorganic–organic heterostructures, such as SiO_2/CD,[7] Fe_2O_3/CD[8] and ZnO/CD[9] for photocatalytic dye degradation, and the organic–organic hybrids, like fluorescent CDs/poly(methyl methacrylate) microbeads.[10] However, most of these CD-loaded nanocomposites are realized by physically blending without chemical coupling, which, despite rare studies, may lead to poor performance. Alternatively, the fabrication of CDs often involves expensive precursors, *e.g.* graphene,[11] or unfriendly chemicals,[12–14] thus limiting their commercial application. In this regard, some cheap or free natural materials, for instance, chicken egg,[15] orange juice,[16] soy milk,[17] pomelo peel,[18] plant leaves[19] and grass,[20] have been adopted as the carbon precursors, providing green and inexpensive access to CDs.

Interestingly, owing to their favourable upconversion photoluminescence (PL) and electron transfer properties, CDs are capable of enhancing the photocatalytic behaviours for some frequently used photocatalysts,[21,22] *e.g.* TiO_2, which always suffer from low efficiency due to their poor light harvesting in the UV range (accounting for 4–5% in the whole solar spectrum).[23–26] Specifically, CDs have been utilized to improve photocatalytic hydrogen generation from water splitting, one of the promising ways to solve the increasing worldwide pollution and energy crisis.[27] Kang *et al.* were the first to demonstrate that graphite-derived CDs are able to improve the photoelectrochemical H_2 generation performance on TiO_2 nanoarrays.[28] Cui and colleagues also presented an impregnation method to combine TiO_2 with CDs for better photocatalytic H_2 production rate.[29] Our group previously described a one-step synthesis of TiO_2/CD nanocomposites from bidentate complexes of TiO_2/vitamin C to boost the photocatalytic H_2 evolution.[30]

In this paper, we present a simple and eco-friendly synthesis of CDs from vegetables including guava, red pepper, peas and spinach. The as-obtained CDs exhibit evident PL emission peaks at around 470 nm, with the PL intensities dependent on the solution concentrations. Typically, the spinach-extracted CDs display the highest PL intensity, which were further integrated with TiO_2 nanoparticles (NPs) and nanotubes (NTs) by hydrothermal synthesis to form well-defined heterostructured nanocomposites. The photocatalytic H_2 evolution performances were explored at different amounts of CD loading, which show a nearly 22-fold higher H_2 rate. We attribute the improvement of H_2 production performance to the favorable electron transfer property of CDs. The extraction of nanomaterials from natural

[a]*Department of Electrical and Computer Engineering, National University of Singapore, 4 Engineering Drive 3, 117576, Singapore. E-mail: elehgw@nus.edu.sg*
[b]*Engineering Science Programme, National University of Singapore, 9 Engineering Drive 1, 117575, Singapore*
[c]*Institute of Materials Research and Engineering, A*STAR (Agency for Science, Technology and Research), 3 Research Link, 117602, Singapore*

precursors, coupled with a convenient strategy to fabricate nanocomposites, may pave an alternative way of producing a large variety of functional materials.

Experimental

Materials

Fresh guava, red pepper, peas and spinach were purchased from local markets, which were washed carefully and cut into pieces ($\sim 1 \times 1$ cm^2) prior to use. The commercial TiO_2 powder, also known as P25 (with an average particle size of $\sim$21 nm), was purchased from Degussa. Ethanol and sodium hydroxide were purchased from standard sources. All the chemicals were used as received without further purification.

Synthesis of pure carbon dots

4 g precursors and 25 mL de-ionized (DI) water were added into a 50 mL Teflon-lined stainless steel autoclave and maintained at 180 °C for 4 h. After the reaction, the autoclave was naturally cooled down to room temperature, yielding a dark brown solution. The solution was centrifuged at 10 000 rpm for 15 min to remove larger particles. The supernatant containing CDs was then collected and filtered with an ultra-filtration membrane (0.2 μm). The CDs solution was dried at 55 °C for 5 h and was re-dispersed in DI water for further use.

Synthesis of TiO_2 nanotubes (NTs)

TiO_2 NTs were synthesized using a hydrothermal method as previously reported.[31] Typically, 1 g P25 powder was added into 35 mL of NaOH solution (10 M) and stirred for 30 min. The suspension was transferred to a 50 mL Teflon-lined autoclave and maintained at 130 °C for 16 h. After the autoclave was naturally cooled down to room temperature, the suspension was collected and then washed repeatedly with HCl (0.1 M) until the pH $\leq$ 1 and further with DI water until the pH $\leq$ 7. The suspension was centrifuged at 10 000 rpm for 10 min and dried at 55 °C overnight to obtain the precipitate. Finally, a soft white powder was achieved after grinding with an agar mortar and calcination at 450 °C for 2 h in a muffle furnace (ramp rate: 5 °C h^{-1}).

Synthesis of TiO_2/CD nanocomposites

A two-step hydrothermal approach was adopted for the synthesis of TiO_2/CD nanocomposites. For the zero-dimensional (0D) composite structure, 0.3 g P25 powder was added into 25 mL of the as-synthesized CDs solution. For the one-dimensional (1D) composite structure, 0.1 g of as-synthesized TiO_2 NTs was added into 25 mL of the CDs solution. Next, the above suspensions were made up to 25 mL with DI water. The mixture was transferred into a 50 mL Teflon-lined stainless steel autoclave and maintained at different temperatures and for different durations. After the reaction, the as-obtained suspension was centrifuged at 10 000 rpm for 5 min. The precipitates were collected respectively and dried in an oven at 55 °C for 4 h for further use.

Photocatalytic water splitting

5 mg TiO_2/CD nanocomposites, 9 mL DI water and 1 mL methanol were mixed in a quartz vial and stirred for 30 min to form a homogeneous suspension. Prior to photocatalytic water splitting, the suspension was purged with argon gas for 10 min. The measurements of H_2 evolution were carried out by magnetically stirring under illumination from a 300 W Xe lamp, and the readings were taken every 30 min over 2 h.

Photocurrent test of photoelectrochemical (PEC) cells

The PECs were realized by coating a layer of glycol suspensions of pure TiO_2 and TiO_2/CD nanocomposites on a FTO glass (1.5×2 cm^2) and drying at 55 °C. With the samples as working electrodes and Pt as the counter electrode, the amperometric *I–t* curves were recorded under illumination of 300 mW cm^{-2} for three 60 s light-on/off cycles without any applied bias.

Characterizations

Fourier transform infrared (FT-IR) spectra of TiO_2 and TiO_2/CD nanocomposites powder were recorded on a Shimadzu IRPrestige-21 FT-IR spectrophotometer. High-resolution transmission electron microscopy (HRTEM) images of the CDs and TiO_2/CD nanocomposites solutions (1 wt%) were taken on a Philips CM300 transmission electron microscope. X-ray diffraction (XRD) spectra of the powder samples were achieved on a Philips X-ray diffractometer with Cu Kα radiation (λ = 1.541 Å). UV-vis absorption spectra were obtained on a Shimadzu UV-3600 UV-vis spectrophotometer. Photoluminescence (PL) spectra were measured on a Shimadzu RF-5301PC spectrofluorophotometer at ambient conditions. X-ray photoelectron spectroscopy (XPS) spectra were attained on a VG Thermo Escalab 220I-XL system. H_2 uptake was measured using pressure composition isotherm measurement on a Shimadzu GC-2014AT gas chromatographer.

Results and discussion

Four types of vegetables, namely guava, red pepper, peas and spinach, abundant in the elements of carbon, nitrogen and oxygen, were selected as the green and natural precursors for the fabrication of CDs. After hydrothermal treatment, some yellow or light brown solutions are achieved, implying the formation of CDs. Fig. 1 shows the PL emission spectra of these vegetable-derived CD solutions at different concentrations of 5, 2.5, 1.25, 0.63, 0.31 and 0.08 mg mL^{-1}. All the CD solutions exhibit evident PL emission peaks centering around 470 nm, with a slight shift of 20 nm in cases of different concentrations (Fig. 1 inset). Although the fluorescence mechanism remains unclear, the PL property of CDs might be associated with their quantum effect and emissive traps on the CD surfaces.[32,33] Moreover, the intensity of these PL emissions is found to be affected by the CD concentrations. In general, PL intensities increase with the CD concentrations at relatively low concentrations until reaching a plateau, similar to the previously reported case,[34] and then decrease at higher concentrations. This can be explained by the so-called "concentration

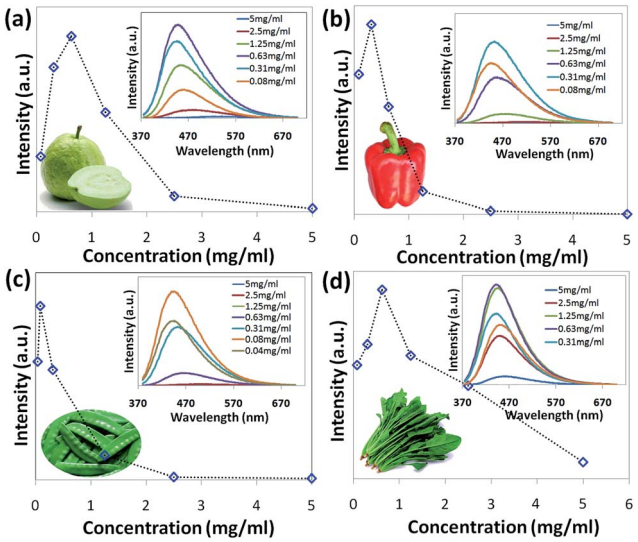

Fig. 1 PL emission trends of the CD solutions at various concentrations extracted from (a) guava, (b) red pepper, (c) peas and (d) spinach. Insets show their respective PL emission spectra at different concentrations.

quenching effect", since the average distances between the luminescent centers are narrowed, leading to unfavorable energy transfer.[35]

We compared the highest PL intensities of the as-derived CD solutions at the optimal solution concentration, as shown in Fig. 2a. The spinach-extracted CDs (the red curve) are observed to display the highest PL emission intensity at a concentration of 0.63 mg mL^{-1}, and these are employed for further exploration and utilization. Fig. 2a inset shows digital photographs of the spinach-extracted CD solution, indicating that the CDs are highly water-soluble. The dispersion displays a dark yellow solution under daylight and a blue emission under laser excitation (λ_{ex} = 400 nm), which visibly confirms the fluorescence characteristics of CDs. Indeed, several functional groups exist on the surfaces of CD nanoparticles, as shown in the FT-IR spectrum (Fig. 2b). To be specific, 3200–3600 cm^{-1} and 1050–1150 cm^{-1} suggest the presence of alcohol O–H and C–O stretch, respectively. The amine N–H stretch band (3300–3500 cm^{-1}) originates from the nitrogen content of the spinach. The presence of these functional groups would impart hydrophilicity to the CDs, rendering them with good solubility in water. Moreover, the aromatic C=C stretch (1400–1600 cm^{-1}) with high sp^2 characteristics contributes to the fluorescence of the CDs due to the π–π^* transition.[36] TEM image (Fig. 2c) shows the spinach-extracted CDs have an average diameter of ~10 nm, with the interplanar lattice spacings of 0.204 nm that reveal the crystalline graphitic carbon. Finally, as seen from the UV-vis spectrum (Fig. 2d), these CDs exhibit an absorption peak at 270 nm that is derived from the aromatic π–π^* system, and also another absorption peak at 320 nm, which should be associated with the characteristic of graphene quantum dots.[37] The CDs also show excitation-dependent PL emissions ranging from 440 to 610 nm, in which the PL emission peaks shift to longer wavelengths as the excitation wavelength increases, along with a decrease in their PL intensities. It is noted that the excitation-dependent emission may be associated with the anti-Stokes photoluminescence of CDs.[38] With the apparent characteristic features displayed by the obtained CDs, the successful fabrication of the vegetable-extracted CDs has been validated.

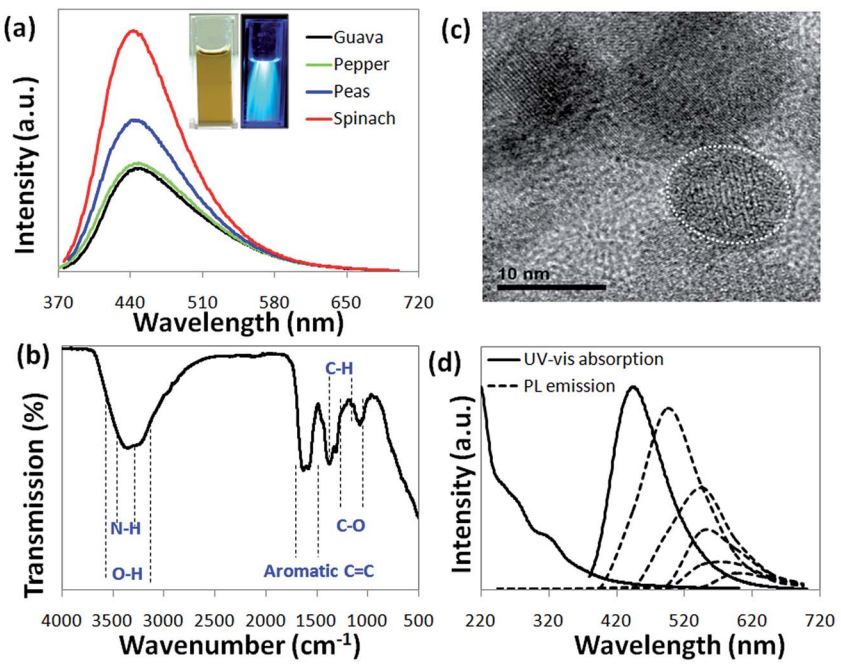

Fig. 2 (a) Optimized PL emission spectra of CDs from different carbon precursors. Inset shows the CD solution under (left) daylight and (right) a 400 nm laser excitation. (b) FT-IR spectrum, (c) TEM image and (d) UV-vis and PL emissions spectra of spinach-derived CDs.

Subsequently, the spinach-extracted CDs are integrated with TiO_2 in different ensembles, including 0D nanoparticles (NPs) and 1D nanotubes (NTs), by further hydrothermal synthesis, in order to form desirable nanocomposites. Fig. 3a and b are the TEM images of the as-prepared TiO_2 NP/CD nanocomposites, in which CD-coated TiO_2 heterostructures are observed. The lattice spacings of 0.35 nm correspond to the anatase (101) facet of TiO_2, while 0.21 nm corresponds to the (100) facet of the CDs. The TEM images of TiO_2 NT/CD nanocomposites are displayed in Fig. 3c and d. Well-defined hollow tube-like structures are clearly seen for the TiO_2 NTs, with a fairly uniform diameter of *ca.* 10 nm (Fig. 3c). At higher magnification, TiO_2 NTs are confirmed by the lattice spacing of 0.35 nm as above, with inner diameter of *ca.* 3.8 nm and wall thickness of *ca.* 1.7 nm. Unlike pure CDs, carbon nanoparticles in the NT/CD composites show lattice spacing of 0.38 nm that corresponds to the (002) facet of CDs, which can be categorized as turbostratic carbon, generally regarded as a variant of hexagonal graphite.[39]

Phase structures and chemical compositions of TiO_2 NPs and NTs with and without CD loading are explored. In Fig. 4, the XRD spectra indicate a mixture of anatase and rutile TiO_2 phases of NPs (the black curve), while the NTs spectrum show the anatase phase (the green curve). TiO_2 NTs are formed by rolling up multiple layers of delaminated anatase sheets owing to energetic factors like surface energy reduction, thereby leading to the pure anatase phase.[40] As for the nanocomposites (red and blue curves), the absence of the (002) carbon peaks at approximately 26° is possibly due to the minute loading of CDs.[41] In the typical XPS spectra of TiO_2 NT/CD nanocomposites (Fig. 4b–d), the binding energies at 284.6 eV, 285.9 eV and 288.3 eV in the C 1s spectra can be assigned to C–C/C=C bond, C–O and C=O bond, respectively. Ti 2p spectra show the peaks at 464.6 and 458.4 eV, which correspond to Ti $2p_{1/2}$ and Ti $2p_{3/2}$, respectively. These values show a slight shift compared to pure TiO_2 (458.1 eV and 463.7 eV), suggesting the combination of

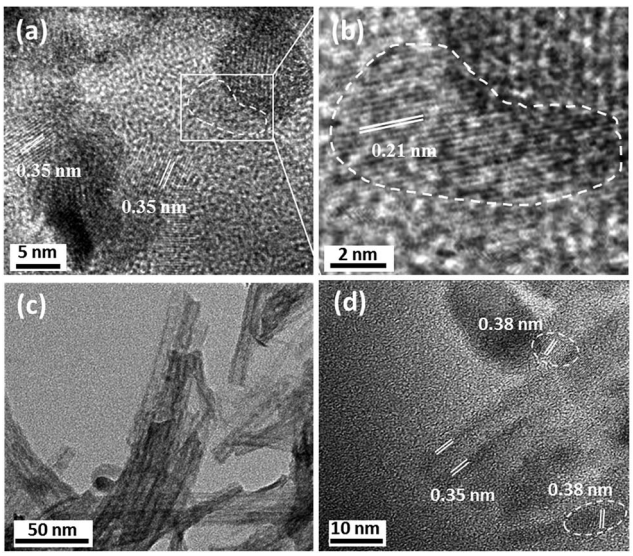

Fig. 3 TEM images of (a and b) TiO_2 NPs and (c and d) NTs composited with spinach-extracted CDs.

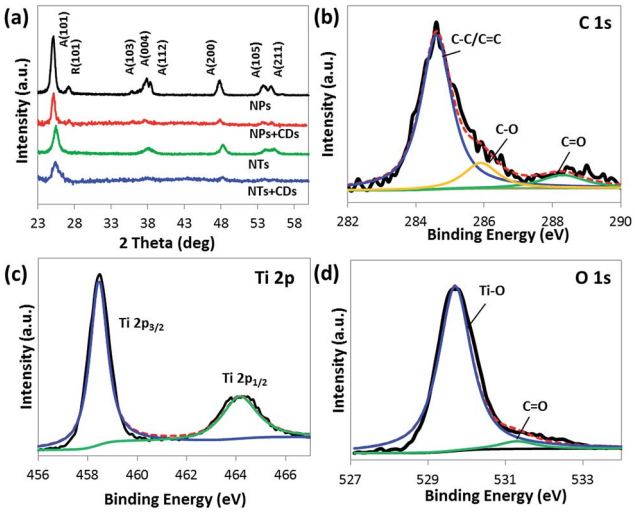

Fig. 4 (a) XRD spectra of TiO_2 NPs and NTs with their CD-loaded nanocomposites. (b) C 1s, (c) Ti 2p and (d) O 1s XPS spectra of TiO_2 NT/CD nanocomposites.

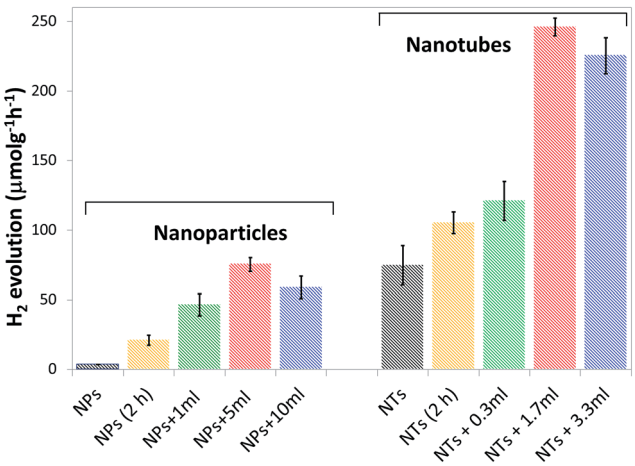

Fig. 5 H_2 evolution rates of TiO_2 NPs, TiO_2 NTs and their nanocomposites loaded with different amounts of CDs.

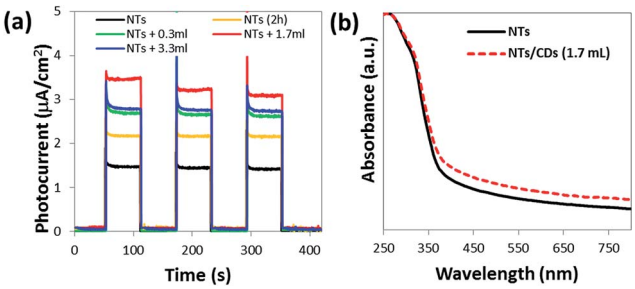

Fig. 6 (a) Photocurrent responses of the PEC cells for three light on/off cycles of TiO_2 and NT/CD nanocomposites. (b) UV-vis absorption spectra of TiO_2 nanotube and its nanocomposites (loaded with 1.7 mL CDs).

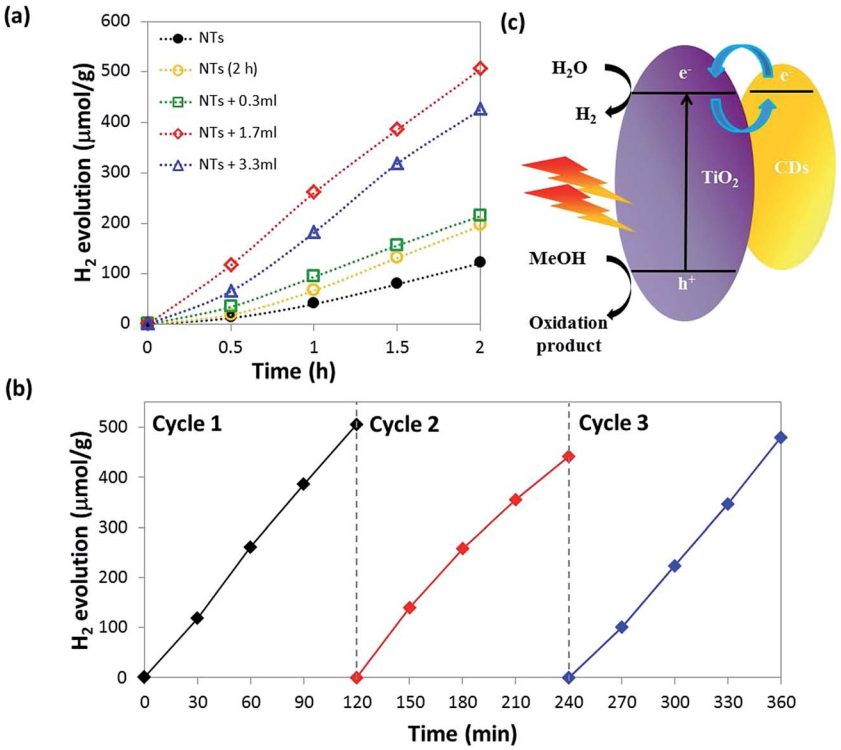

Fig. 7 (a) H_2 production of NTs and their nanocomposites at different CD loadings. (b) H_2 production cycling of NTs with 1.7 mL CDs. (c) Schematic illustration of the proposed photocatalytic mechanism.

CDs with TiO_2. The O 1s spectra exhibit two peaks at 529.7 and 531.4 eV, which are attributed to Ti–O and C=O groups, respectively. Notably, a Ti–C peak (~281 eV) was not found in either Ti 2p or C1s spectra, suggesting that CDs are integrated rather than doped into the TiO_2 nanostructures.

The as-attained TiO_2 NP/CD and NT/CD nanocomposites are evaluated as photocatalysts for solar H_2 production from sacrificial water splitting. Fig. 5 shows the H_2 evolution rates of bare TiO_2 NPs, NTs and their nanocomposites loaded with different amounts of CDs, respectively. In principle, the CD-loaded nanocomposites exhibit better H_2 generation performance than bare TiO_2 (3.5 μmol g^{-1} h^{-1} for NPs and 74.8 μmol g^{-1} h^{-1} for NTs), which might be ascribed to the enhanced electron charge transfer between CDs and TiO_2 host photocatalysts. In both cases, the H_2 evolution rates increased with the CD loading amounts until reaching the highest (the red bars), but decreased beyond the optimal CD loading concentrations (the blue bars). To be specific, the H_2 rate reaches 75.5 μmol g^{-1} h^{-1} when loaded with 5 mL CDs, which is 21.6 times higher than bare TiO_2 NPs, and 246.1 μmol g^{-1} h^{-1} at 1.7 mL CD loading, 3.3 times higher than bare NTs. However, excessive CD loading (10 mL for NPs and 3.3 mL for NTs) will cause detrimental photocatalytic behavior with decreased H_2 evolution rate, probably due to the blocking of TiO_2 from light irradiation.[30,42] Overall, TiO_2 NTs and their nanocomposites perform higher H_2 rates than TiO_2 NPs, which is attributed to the distinct 1D structure and phase of the nanotubes. On one hand, NTs are able to enhance the charge conductivity, allowing the generated electron–hole pairs to effectively transport longitudinally along the unique 1D structure. On the other hand, NTs possess a pure anatase phase rather than the mixture of both anatase and rutile phases in NPs, as determined from the XRD spectra above. The anatase phase is ideal for the photocatalytic behavior for TiO_2 because of its longer charge carrier life time and mitigated recombination of electron–hole pairs.[43] It is noted that the hydrothermal treatment can also enhance the H_2 rate of TiO_2 (the yellow bar), since the hydroxyl groups on the TiO_2 surfaces are increased, which partially mediates the charge transport.[44]

Furthermore, the typical photoelectrochemical (PEC) responses of TiO_2 NTs and NT/CD nanocomposites are recorded. The two-electrode PEC cells are achieved using bare TiO_2 NTs or NT/CD nanocomposites as the working electrodes, with their amperometric *I–t* curves obtained at three light on/off cycles within 60 s, as shown in Fig. 6a. The photocurrent measurements are consistent over the three on/off cycles, demonstrating the stability of NTs and their nanocomposites. The photocurrent densities of all the nanocomposites are higher than the pristine NTs (1.48 μA cm^{-2}), with the sample loaded with 1.7 mL of CDs reaching the highest density at 3.46 μA cm^{-2}. It is believed that higher photocurrent density would indicate a slower electron–hole pair recombination rate, which is favorable for photocatalytic H_2 production.[45] A decrease in the photocurrent density as CDs increase to 3.3 mL can also be attributed to excessive CD loading, which shields the absorption of incident light. The trend is similar to the H_2

generation rates for the nanocomposites loaded with different amounts of CDs, suggesting the electron–hole separation plays a significant role in the whole photocatalytic process. The UV-vis absorption spectra of NTs and NT/CD nanocomposites (1.7 mL CDs loading) are also obtained for comparison (Fig. 6b). It is seen that the loading of CDs enhances light absorption of NTs at wavelengths over 385 nm. Moreover, a slight increase in absorption edge is observed, indicating the NT/CD nanocomposites are able to utilize a wider range of the solar spectrum for enhanced photocatalytic H_2 production.

The detailed H_2 evolution trends of TiO_2 NTs with and without CD loading are presented in Fig. 7a, in which the relatively linear graphs demonstrate constant H_2 production without photodegradation or saturation. To showcase the stability of NT/CD nanocomposites, H_2 evolution was measured for two hours over three cycles (Fig. 7b), in which the H_2 evolution rates are relatively stable without obvious fluctuation. A possible mechanism for the enhanced photocatalytic H_2 production is proposed in Fig. 7c. First, CDs are reported to serve as benign electron acceptors and donors, leading the photoinduced electrons to transfer from CDs to TiO_2 surfaces and the redundant electrons on TiO_2 to the CD particles during the photocatalytic process.[46] As a result, the electron–hole pair recombination is greatly prohibited between TiO_2 and CDs, as also evidenced from the photocurrent densities. Second, the extension of UV-vis absorption edge with the introduction of CDs should allow effective utilization of the solar spectrum for TiO_2, leading to improved photocatalytic performance.

Conclusions

In summary, we present an easy and available hydrothermal method for the synthesis of TiO_2/CD nanocomposites for photocatalytic purposes. Water-soluble CDs with favorable photoluminescent properties are extracted from cheap and green vegetables, ensuring the non-toxicity of the final products. Typically, the spinach-derived CDs exhibit favorable PL emission intensity and good UV absorption characteristics, and the presence of an amine functional group allows CDs to be bonded to TiO_2 surfaces without post surface modification. These nanocomposites demonstrated great enhancement of photocatalytic H_2 evolution, as the loaded CDs extended the UV absorption range and reduced the electron–hole pair recombination. At optimal CD loading concentration, the H_2 evolution rate reached 75.5 and 246.1 μmol g^{-1} h^{-1}, which are 21.6 and 3.3 times higher than for pure NTs and NPs, respectively. The easy and green method may contribute to the facile fabrication of benign nanocomposites for diverse applications.

Acknowledgements

This work is supported by the National University of Singapore (NUS) grant R-263-000-653-731/654-112 and A*STAR R-263-000-A96-305.

Notes and references

1 M. Zhu and G. Diao, *Nanoscale*, 2011, **3**, 2748–2767.
2 H. Kim, A. A. Abdala and C. W. Macosko, *Macromolecules*, 2010, **43**, 6515–6530.
3 D. S. Su and R. Schlögl, *ChemSusChem*, 2010, **3**, 136–168.
4 Y.-P. Sun, B. Zhou, Y. Lin, W. Wang, K. A. S. Fernando, P. Pathak, M. J. Meziani, B. A. Harruff, X. Wang, H. Wang, P. G. Luo, H. Yang, M. E. Kose, B. Chen, L. M. Veca and S.-Y. Xie, *J. Am. Chem. Soc.*, 2006, **128**, 7756–7757.
5 S. N. Baker and G. A. Baker, *Angew. Chem., Int. Ed.*, 2010, **49**, 6726–6744.
6 H. Zhu, X. Wang, Y. Li, Z. Wang, F. Yang and X. Yang, *Chem. Commun.*, 2009, 5118–5120.
7 H. Li, X. He, Z. Kang, H. Huang, Y. Liu, J. Liu, S. Lian, C. H. A. Tsang, X. Yang and S.-T. Lee, *Angew. Chem.*, 2010, **122**, 4532–4536.
8 H. Zhang, H. Ming, S. Lian, H. Huang, H. Li, L. Zhang, Y. Liu, Z. Kang and S.-T. Lee, *Dalton Trans.*, 2011, **40**, 10822–10825.
9 H. Yu, H. Zhang, H. Huang, Y. Liu, H. Li, H. Ming and Z. Kang, *New J. Chem.*, 2012, **36**, 1031–1035.
10 S.-S. Liu, C.-F. Wang, C.-X. Li, J. Wang, L.-H. Mao and S. Chen, *J. Mater. Chem. C*, 2014, **2**, 6477–6483.
11 D. Pan, J. Zhang, Z. Li and M. Wu, *Adv. Mater.*, 2010, **22**, 734–738.
12 H. Jiang, F. Chen, M. G. Lagally and F. S. Denes, *Langmuir*, 2010, **26**, 1991–1995.
13 A. B. Bourlinos, A. Stassinopoulos, D. Anglos, R. Zboril, M. Karakassides and E. P. Giannelis, *Small*, 2008, **4**, 455–458.
14 F. Wang, S. Pang, L. Wang, Q. Li, M. Kreiter and C.-Y. Liu, *Chem. Mater.*, 2010, **22**, 4528–4530.
15 J. Wang, C.-F. Wang and S. Chen, *Angew. Chem., Int. Ed.*, 2012, **51**, 9297–9301.
16 S. Sahu, B. Behera, T. K. Maiti and S. Mohapatra, *Chem. Commun.*, 2012, **48**, 8835–8837.
17 C. Zhu, J. Zhai and S. Dong, *Chem. Commun.*, 2012, **48**, 9367–9369.
18 W. Lu, X. Qin, S. Liu, G. Chang, Y. Zhang, Y. Luo, A. M. Asiri, A. O. Al-Youbi and X. Sun, *Anal. Chem.*, 2012, **84**, 5351–5357.
19 S. Liu, J. Tian, L. Wang, Y. Zhang, X. Qin, Y. Luo, A. M. Asiri, A. O. Al-Youbi and X. Sun, *Adv. Mater.*, 2012, **24**, 2037–2041.
20 L. Zhu, Y. Yin, C.-F. Wang and S. Chen, *J. Mater. Chem. C*, 2013, **1**, 4925–4932.
21 H. Li, Z. Kang, Y. Liu and S.-T. Lee, *J. Mater. Chem.*, 2012, **22**, 24230–24253.
22 B. Y. Yu and S.-Y. Kwak, *J. Mater. Chem.*, 2012, **22**, 8345–8353.
23 M. Gao, C. K. N. Peh, W. L. Ong and G. W. Ho, *RSC Adv.*, 2013, **3**, 13169–13177.
24 M. Ye, J. Gong, Y. Lai, C. Lin and Z. Lin, *J. Am. Chem. Soc.*, 2012, **134**, 15720–15723.
25 M. Wang, L. Sun, Z. Lin, J. Cai, K. Xie and C. Lin, *Energy Environ. Sci.*, 2013, **6**, 1211–1220.
26 M. Wang, J. Loccozia, L. Sun, C. Lin and Z. Lin, *Energy Environ. Sci.*, 2014, **7**, 2182–2202.
27 X. Chen, S. Shen, L. Guo and S. S. Mao, *Chem. Rev.*, 2010, **110**, 6503–6570.

28 X. Zhang, F. Wang, H. Huang, H. Li, X. Han, Y. Liu and Z. Kang, *Nanoscale*, 2013, **5**, 2274–2278.
29 M. Sun, X. Ma, X. Chen, Y. Sun, X. Cui and Y. Lin, *RSC Adv.*, 2014, **4**, 1120–1127.
30 J. Wang, M. Gao and G. W. Ho, *J. Mater. Chem. A*, 2014, **2**, 5703–5709.
31 S. D. Perera, R. G. Mariano, K. Vu, N. Nour, O. Seitz, Y. Chabal and K. J. Balkus Jr, *ACS Catal.*, 2012, **2**, 949–956.
32 Z.-A. Qiao, Y. Wang, Y. Gao, H. Li, T. Dai, Y. Liu and Q. Huo, *Chem. Commun.*, 2010, **46**, 8812–8814.
33 L. Zheng, Y. Chi, Y. Dong, J. Lin and B. Wang, *J. Am. Chem. Soc.*, 2009, **131**, 4564–4565.
34 D. Pan, L. Guo, J. Zhang, C. Xi, Q. Xue, H. Huang, J. Li, Z. Zhang, W. Yu, Z. Chen, Z. Li and M. Wu, *J. Mater. Chem.*, 2012, **22**, 3314–3318.
35 G. H. Mhlongo, M. S. Dhlamini, H. C. Swart, O. M. Ntwaeaborwa and K. T. Hillie, *Opt. Mater.*, 2011, **33**, 1495–1499.
36 D. Pan, J. Zhang, Z. Li, C. Wu, X. Yan and M. Wu, *Chem. Commun.*, 2010, **46**, 3681–3683.
37 S. Zhu, J. Zhang, C. Qiao, S. Tang, Y. Li, W. Yuan, B. Li, L. Tian, F. Liu, R. Hu, H. Gao, H. Wei, H. Zhang, H. Sun and B. Yang, *Chem. Commun.*, 2011, **47**, 6858–6860.
38 J. Shen, Y. Zhu, C. Chen, X. Yang and C. Li, *Chem. Commun.*, 2011, **47**, 2580–2582.
39 Z. Q. Li, C. J. Lu, Z. P. Xia, Y. Zhou and Z. Luo, *Carbon*, 2007, **45**, 1686–1695.
40 T. J. Wong, F. J. Lim, M. Gao, G. H. Lee and G. W. Ho, *Catal. Sci. Technol.*, 2013, **3**, 1086–1093.
41 H. Zhang, H. Huang, H. Ming, H. Li, L. Zhang, Y. Liu and Z. Kang, *J. Mater. Chem.*, 2012, **22**, 10501–10506.
42 J. Wang, Y.-F. Lim and G. W. Ho, *Nanoscale*, 2014, **6**, 9673–9680.
43 M. Xu, Y. Gao, E. M. Moreno, M. Kunst, M. Muhler, Y. Wang, H. Idriss and C. Wöll, *Phys. Rev. Lett.*, 2011, **106**, 138302.
44 J. Yu, H. Yu, B. Cheng, M. Zhou and X. Zhao, *J. Mol. Catal. A: Chem.*, 2006, **253**, 112–118.
45 H. M. Chen, C. K. Chen, R.-S. Liu, L. Zhang, J. Zhang and D. P. Wilkinson, *Chem. Soc. Rev.*, 2012, **41**, 5654–5671.
46 X. Wang, L. Cao, F. Lu, M. J. Meziani, H. Li, G. Qi, B. Zhou, B. A. Harruff, F. Kermarrec and Y.-P. Sun, *Chem. Commun.*, 2009, 3774–3776.